

Changing Snowpack Dynamics:
Phase Predictions and Forest Implications
by
Taylor Scott Winchell
B.S., University of California, Berkeley, 2014

A thesis submitted to the
Faculty of the Graduate School of the
University of Colorado in partial fulfillment
of the requirement for the degree of
Masters of Science
Department of Civil, Environmental, and Architectural Engineering
2016

This thesis entitled:
Changing Snowpack Dynamics: Phase Predictions and Forest Implications
written by Taylor Scott Winchell
has been approved for the Department Civil, Environmental, and Architectural Engineering

Noah Molotch

Balaji Rajagopalan

Ben Livneh

Date _____

The final copy of this thesis has been examined by the signatories, and we find that both the content and the form meet acceptable presentation standards of scholarly work in the above mentioned discipline.

Winchell, Taylor Scott (M.S., Civil Engineering)

Changing Snowpack Dynamics: Phase Predictions and Forest Implications

Thesis directed by Professor Noah P. Molotch

Chapter I Abstract

Previous work demonstrates conflicting evidence regarding the influence of snowmelt timing on forest net ecosystem exchange (NEE). Based on 15 years of eddy-covariance measurements in Colorado, years with earlier snowmelt exhibited less net carbon uptake during the snow-ablation period, which is a period of high potential for productivity. Earlier snowmelt aligned with colder periods of the seasonal air temperature cycle relative to later snowmelt. We found that the colder ablation-period air temperatures during these early snowmelt years lead to reduced rates of daily NEE. Hence, earlier snowmelt associated with climate warming, counter-intuitively, leads to colder atmospheric temperatures during the snow-ablation period and concomitantly reduced rates of net carbon uptake. Using a multilinear-regression ($R^2=0.79$, $P<0.001$) relating snow-ablation period mean air temperature and peak snow water equivalent (SWE) to ablation-period NEE, we predict that earlier snowmelt and decreased SWE may cause a 45% reduction in mid-century ablation-period net carbon uptake.

Chapter II Abstract

Dai [2008] used a 29-year observational precipitation phase dataset to produce global conditional snow frequency curves (frequency of snow events per air temperature bin) for the land and ocean. We extended upon Dai's study to further explore the influence of three physically relevant variables (surface air temperature (T_s), relative humidity (RH), surface

pressure (Ps)) on conditional snow frequency over the land surface. We found that precipitation events that fell at low ambient RH and/or low Ps had greater snow frequencies at high Ts compared with events that fell at high ambient RH and/or high Ps, respectively. However, the range in snow frequencies per Ps class is less than the range per RH class. We developed and compared three binary logistic regression models using Ts, RH and Ps as predictor variables for precipitation phase. The Ts-RH model performed universally better than the simple Ts model and the Ts-RH-Ps model had nearly identical success rates to the Ts-RH model. The largest difference in success rates between the Ts-RH model and the simple Ts model occurred at the lower RH classes, and all models performed universally better in the higher RH classes. Therefore, while our results demonstrate that RH should be included in precipitation phase predictive models whenever possible, we might expect RH to more significantly contribute to models utilized in climatically dry regions. These models were developed and tested with a global dataset of ~15 million precipitation observations and thus present the most the most extensive global phase prediction model to date

Acknowledgements

This material is based upon work supported by the U.S. National Science Foundation (NSF) Graduate Research Fellowship (NSF Grant DGE 1144083), the NSF – U.S. Department of Agriculture (USDA) joint program for Water Sustainability and Climate (USDA Grant: 2012-67003-19802), and the NSF Hydrological Sciences Program (NSF Grant: EAR1141764). Data Collection was funded by the U.S. Department of Energy (DOE), the USDA and the NSF Niwot Ridge Long Term Ecological Research program. The US-NR1 AmeriFlux site is supported by the DOE Office of Science through the AmeriFlux Management Project (AMP) at Lawrence Berkeley National Laboratory under award number 7094866. We offer thanks to Peter Blanken and all others involved in the AmeriFlux data collection efforts.

I would like to thank my advisor, Prof. Noah Molotch, along with the entirety of the mountain snow hydrology research group for providing an atmosphere that fosters learning, innovative and diverse research, and lasting camaraderie. Prof. Ben Livneh and Prof. Balaji Rajagopalan have additionally provided incredible support, ideas, and inspiration both in my research and general life pursuits. My parents, Clark and Jill Winchell, have inspired me every day with an unwavering foundation of support, understanding and encouragement. My dog, Ellie, has never let me forget the importance of a walk around the block. Lastly, I am forever grateful to have been lucky enough to spend my time in graduate school working in the same building as my brother, inspiration and friend, Eric Winchell.

Contents

Chapter I.

Introduction.....	1
Data & Methods.....	3
Results.....	6
Discussion.....	13
Conclusion.....	16

Chapter II.

Introduction.....	18
Data & Methods.....	20
Results.....	25
Discussion.....	30
Conclusion.....	32

References.....	34
-----------------	----

Appendix A.....	37
-----------------	----

Tables

Chapter II

1. Precipitation observations per relative humidity class.....	22
2. Precipitation observations per pressure class.....	22
3. Model coefficients	30
4. Model success rates.....	30

Appendix A

A1. Niwot Ridge AmeriFlux and SnoTel data (1999-2013)	39
---	----

Figures

Chapter I

1. Snow water equivalent and air temperature seasonal cycles7
2. Snow water equivalent – melt timing – air temperature relationships.....9
3. Ablation period NEE model output results 11
4. Ablation period NEE to full season NEE analysis.....13

Chapter II

1. Global station distribution.....21
2. Temperature precipitation frequency per relative humidity class.....26
3. Snow frequency per relative humidity class27
4. Temperature precipitation frequency per pressure class.....28
5. Snow frequency per pressure class29

Appendix A

- A1. PPFD vs. ablation period daily NEE.....37
- A2. Melt timing vs. full-season NEE.....38

Chapter I: Early Snowmelt Reduces Atmospheric Carbon Uptake in Coniferous Forests

Introduction

Globally, forests represent a large and persistent terrestrial carbon sink that regulates atmospheric CO₂ concentration [Pan *et al.*, 2011]. Forty percent of these forests reside in seasonally snow-covered environments, which are particularly sensitive to climate change due to the temperature dependence of precipitation phase [Barnett *et al.*, 2005; Flanner *et al.*, 2011]. Seasonally snow-covered forests represent a key terrestrial carbon sink in both mountainous [Schimel *et al.*, 2002] and boreal ecosystems [Bernhardt and Schlesinger, 2013]. Evaluating the climate sensitivity of these forests is critical as winter temperatures are increasing [Baldwin *et al.*, 2003; Bradley, 2004; Nogués-Bravo *et al.*, 2007], causing reductions in snow accumulation [Hamlet *et al.*, 2005; Mote, 2006; Clow, 2010] and shifting snowmelt earlier in the year [Stewart *et al.*, 2004; Clow, 2010].

The snow-ablation period, which provides a sustained soil water input, is a time of great potential for carbon uptake in seasonally snow-covered environments [Monson *et al.*, 2005; Harpold and Molotch, 2015]. In evergreen mountain forests, where carbon uptake is biophysically restrained during the winter, the snow-ablation period is when the ecosystem begins to assimilate carbon through photosynthesis and relatively low soil temperatures diminish carbon loss from soil respiration [Monson *et al.*, 2005]. As a result, carbon uptake during the snow-ablation period can account for a significant component of growing season NEE (up to 42% [Monson *et al.*, 2005]). However, varying meteorological conditions can impact carbon uptake rates during this time [Huxman *et al.*, 2003].

Synthesis studies of atmospheric carbon uptake in forested ecosystems, including those from mountain and high-latitude sites, have predicted that earlier springs and later autumns, due to climate warming, will result in increased carbon sequestration [Richardson *et al.*, 2010]. However, several reports have blurred our understanding of the direction (source or sink) and magnitude of forest-atmosphere CO₂ exchange in the face of climate variation. Some studies of high-latitude forests have revealed increased [Black *et al.*, 2000], decreased [Goulden, 1998], or no effect [Dunn *et al.*, 2007] of earlier spring snow melt on total seasonal forest carbon uptake. Piao *et al.* [2008] and Wu *et al.* [2013] have shown that the effects of earlier spring warming and snowmelt on high-latitude forest net carbon exchange is dictated by the relative magnitudes of increased seasonal photosynthetic uptake versus increased autumn respiration. Similar photosynthesis-respiration trade-offs are at play in subalpine forests, as some studies show that longer growing seasons lead to less carbon uptake [Sacks *et al.*, 2007; Hu *et al.*, 2010], while others indicate the contrary [Scott-Denton *et al.*, 2013; Mitchell *et al.*, 2015]. We note that these seasonally snow covered high-latitude and subalpine forests share similar dependencies on snowmelt as a water source and both have a general energy limitation during the winter; however, they differ in their species compositions and meteorological conditions (e.g. given latitudinal gradients in solar radiation).

Given the lack of consensus regarding the carbon balance response to changing snowmelt timing, it is important to determine whether seasonally snow-covered forest carbon sinks are strengthened or weakened in response to climate warming. We examined relationships between net ecosystem exchange (NEE) eddy covariance measurements and observed snow water equivalent (SWE) in a mid-latitude subalpine forest. Our objective is to characterize the

productivity response of subalpine forest ecosystems to hydrometeorological conditions during the snow-ablation period and to predict future productivity given changes in snowmelt timing and accumulation associated with climate warming.

Data and Methods

a) Site Description

This study was conducted at the Niwot Ridge AmeriFlux site US-NR1, a subalpine forest in the Colorado Rocky Mountains at an elevation of 3050 m located 8 km east of the Continental Divide (40°1' 58"N 105°32' 47"W). The subalpine forest ecosystem (LAI=4.2 m²/m²; canopy height=11.5 m) is dominated by subalpine fir (*Abies lasiocarpa*), Engelmann spruce (*Picea engelmannii*), and lodgepole pine (*Pinus contorta*). Mean-annual precipitation is approximately 800 mm, with about 65% in the form of snow. Mean annual temperature is 1.5°C. Descriptions of the physical and meteorological characteristics of the site can be found in previous studies [Monson *et al.*, 2002, 2005; Turnipseed *et al.*, 2002, 2003].

b) Eddy Covariance and Snow Water Equivalence (SWE) Measurements

NEE has been continuously measured at 30-minute intervals from the 26 m Niwot Ridge AmeriFlux tower since November, 1998. We used 15 years (1999-2013) of AmeriFlux friction-velocity-filtered NEE, gap-filled measurements (ver.2014.12.02). This version includes a correction to an error in the dataset where a water-vapor correction was applied twice during the closed-path IRGA CO₂ flux calculation [Burns *et al.*, 2015]. Full descriptions of the eddy-covariance method used to measure NEE have been previously presented [Monson *et al.*, 2002].

Further information on the turbulent flux gap-filling procedures can be found at:

http://urquell.colorado.edu/data_ameriflux/

Daily SWE measurements were obtained from the Niwot Snowpack Telemetry (SNOTEL) station, located within 500 m of the flux tower (<http://www.wcc.nrcs.usda.gov/nwcc/site?sitenum=663>). We defined both the date and magnitude of peak SWE by the final local maxima in the SWE time-series in which the SWE magnitude is within 95% of the global SWE maxima. Subsequently, we defined the ablation period as the peak SWE date to the day of snow disappearance (SWE=0 m) and analyzed ablation-period daily NEE (cumulative ablation-period NEE divided by the length of the ablation period) in relation to the ablation-period mean air temperature (21.5 m). In this study ‘daytime’ is defined as any period of the day that the photosynthetic photon flux density (PPFD) is greater than 20 $\mu\text{mol}/\text{m}^2/\text{sec}$. We defined the non-ablation period as the date of snow disappearance to the day that the 13-day moving average of NEE switches from negative to positive at the end of the season, indicating a transition from net carbon uptake to net carbon loss. We thus defined a ‘full season’ from the date of peak SWE to the last day of the non-ablation period.

c) Statistical methods and ablation-period NEE model

Previous work in subalpine forests has illustrated NEE sensitivity to air temperature [*Huxman et al.*, 2003; *Monson et al.*, 2005], with maximum light saturated CO_2 uptake occurring at approximately 11°C [*Huxman et al.*, 2003]. A shift in the timing of snowmelt may have large impacts on air temperature during the early part of the growing season – which generally begins at the onset of snowmelt [*Monson et al.*, 2005]. To explore the relationship between the change in the timing of snowmelt and air temperature during the ablation period, we used a linear

regression relating the date of peak SWE and ablation-period mean air temperature. We then explored the relationship between ablation-period mean air temperature and ablation period daily NEE, as well as the relationship between the date of peak SWE and the ratio of ablation-period cumulative NEE to full-season cumulative NEE. We used the relationship between date of peak SWE and ablation-period mean air temperature to produce a linear regression equation which uses the date of peak SWE as a predictor of ablation-period mean air temperature.

To evaluate the processes influencing the range in total ablation-period NEE, we performed a multiple linear regression analysis with ablation-period mean air temperature and peak-SWE magnitude as physical predictors to explain the variation in total ablation-period NEE. These predictor variables were chosen for the multiple linear regression analysis both because of their individual correlations with ablation period NEE and our ability to project future trends of these variables based on current literature. We used the resulting multiple linear regression equation as a model to demonstrate potential current and future scenarios of ablation-period NEE. To obtain the range of temperature values used as model input, we first inputted a range of day of peak SWE values into the linear regression equation established between day of peak SWE and ablation-period mean air temperature. Day of peak SWE inputs ranged from Day of Year (DOY) 65 to DOY 145, as the minimum DOY of peak SWE from the observed record was 73 and the maximum DOY of peak SWE was 144. We then took the resulting temperature range, along with a peak SWE magnitude range of 0.17 m–0.50 m (15-year observed record ranged from 175.3 mm to 454.7 mm), as model inputs to generate a range of potential ablation period NEE values.

Results

The maximum ablation-period length was 55 days (2003) and the minimum was 17 days (2010) (Table A1 – Appendix A). The latest date of peak SWE was 24 May 2011 and the earliest was 13 March 2012, resulting in a substantial range in the date of peak SWE (71 days). Fig. 1 demonstrates that the timing of peak SWE determined the alignment of the ablation period with the seasonal air temperature cycle: an early ablation period (e.g. 2002) occurred during a colder period (mean temperature= 1.9°C) of the seasonal air temperature cycle relative to a later ablation period (e.g. 2013) that occurred during a warmer period (mean temperature= 6.7°C). Thus, we next explored the phenological implications of the ablation timing/temperature alignment for ablation period NEE.

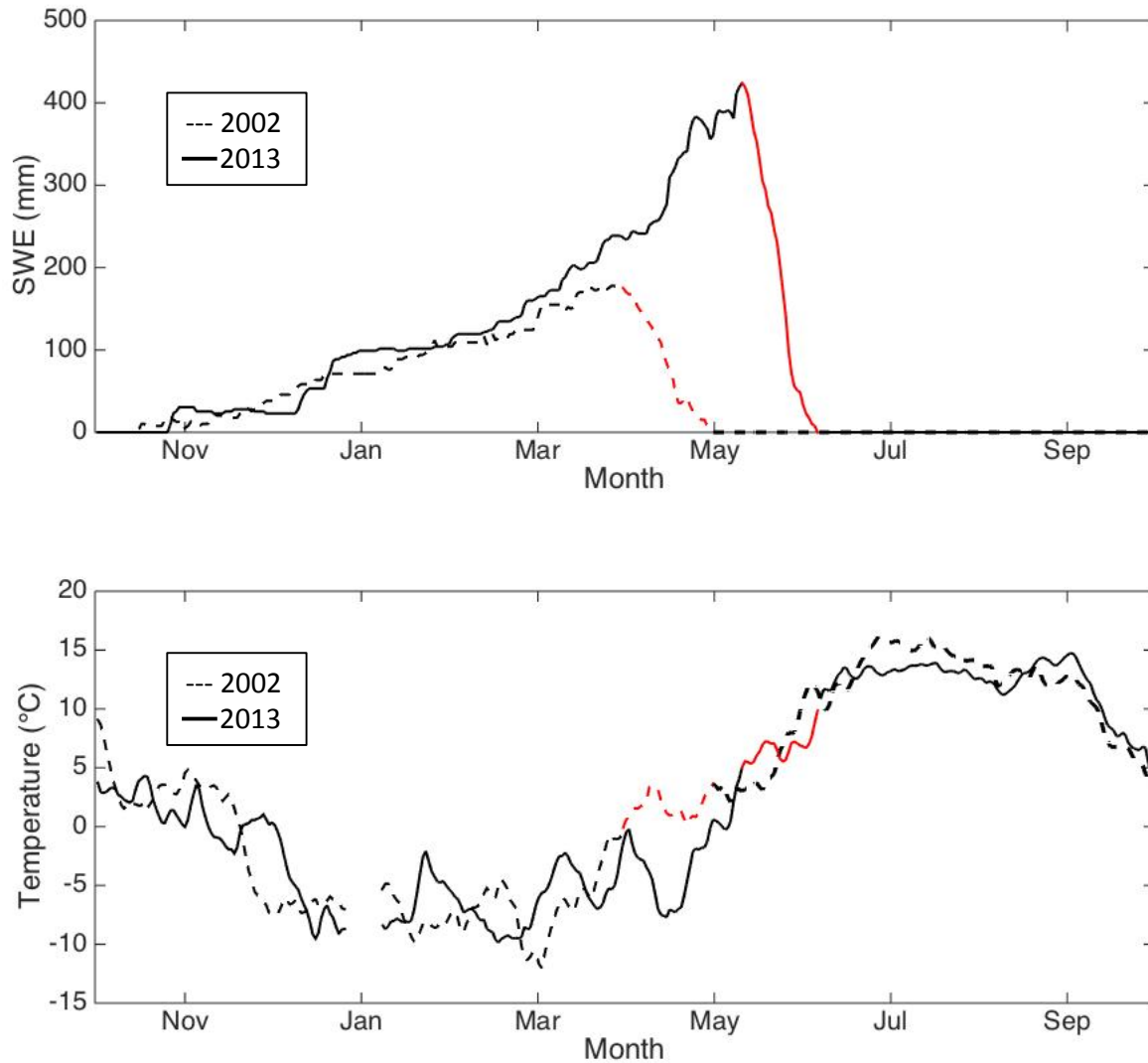


Figure 1 | (a) Snow water equivalent seasonal cycles for an early (WY-2002) and late (WY-2013) ablation period. Red lines distinguish the ablation period. (b) Corresponding air temperature seasonal cycles for WY-2002 and WY-2013. Plotted as the 13-day moving average of daily temperatures. Red lines distinguish the temperatures during the ablation period.

We found that the range in the date of peak SWE resulted in a vast range of ablation period mean air temperatures (1.9–7.9°C). Fig. 2a displays a significant positive correlation ($R^2=0.72$, $P<0.001$) between the date of peak SWE and the ablation-period mean air temperature. This relationship produced the following linear regression equation:

$$(1) \quad T = -4.1662 + 0.07881 * (D)$$

where D is the Day of Year (DOY) of peak SWE. Equation (1) demonstrates that as snow melts earlier, the ablation period experiences mean air temperatures progressively less than the maximum CO₂ uptake rate temperature of 11°C [Huxman *et al.*, 2003], effectively misaligning the period of sustained soil water input from the timing of the optimum net uptake temperature.

We found a significant negative correlation ($R^2=0.87$, $P<0.001$) between ablation period daily NEE and ablation period mean air temperature (Fig. 2b). Lower mean air temperatures corresponded with reduced ablation period daily NEE. The variation in ablation period daily NEE was driven by ablation period daytime NEE, as daytime NEE had a range of 3.78 gC/m²/d, whereas nighttime NEE had a range of only 0.16 gC/m²/d. Example half-hourly data illustrate the NEE sensitivity to snowmelt timing and air temperature whereby NEE rates are shown to increase dramatically from early to late snowmelt (Figure 2c). In comparing NEE between an early ablation period (2002) and the same period during a year with late melt (2013), the daytime NEE rate during the 2002 ablation period (31 March-1 May) was -0.42 gC/m²/d, while the same time period for late ablation year of 2013 (31 March-1 May, before 2013 ablation period begins) reported a daytime NEE rate of 0.29 gC/m²/d. The sign difference in these two daytime NEE quantities indicates that the forest was active during the melt period in 2002, but not during the same time period in 2013 when melt was not occurring. The early ablation example in Fig. 2c further demonstrates the sensitivity of forest NEE to early snow ablation, as we see that there was a sudden reduction in NEE for an approximate 4-day stretch associated with air temperatures below 0°C; these rapid drops in air temperature are less likely to occur later in the year. We note

that we did not find a significant relationship between ablation period daily NEE and ablation-period mean daytime PPFD ($R^2=0.11$, $P=0.23$, supplemental Fig. A1 – Appendix A).

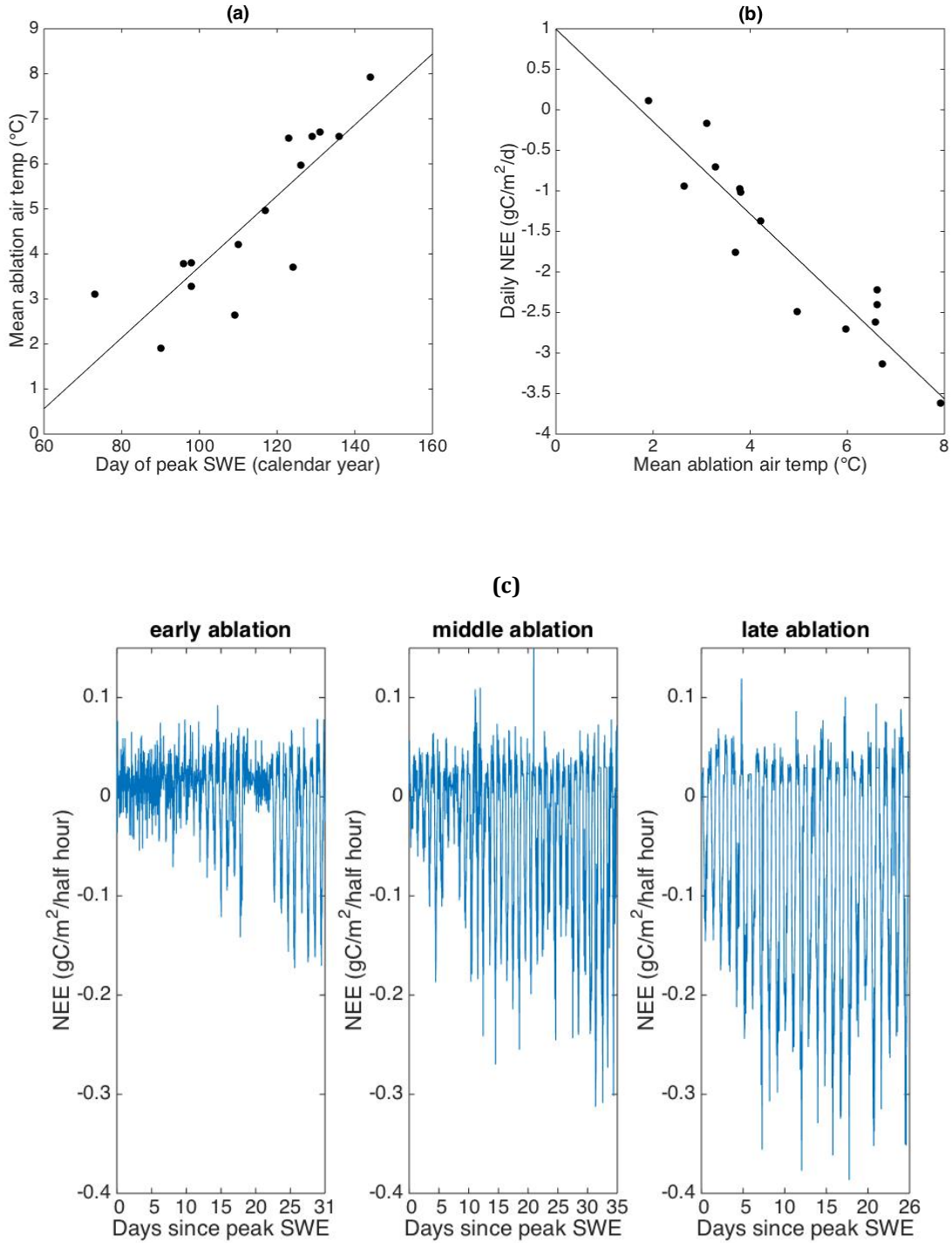


Figure 2 | (a) Relationship between date of peak SWE (horizontal axis) and mean air temperature during the ablation period (vertical axis) ($R^2=0.72$, $P<0.001$). **(b)** Relationship between mean air temperature during the ablation period (horizontal axis) and ablation period daily NEE (vertical axis)($R^2=0.87$, $P<0.001$). **(c)** Half-hourly NEE for the 2002 ablation period that began on 31 March (early ablation), 2009 ablation period that began on 20 April (middle ablation), 2013 ablation period that began on 22 May (late ablation).

The range in ablation period NEE was 95.4 gC/m^2 . In 2002 we observed a positive ablation period NEE (3.36 gC/m^2); the ablation-period mean air temperature (1.9°C) and the peak SWE magnitude (175.3 mm) for 2002 were the respective variable minimums for the 15 year record. Additionally, the 2002 ablation-season mean daytime uptake rate (-0.42 gC/m^2) was the minimum for the period of record. The mean nighttime respiration (0.53 gC/m^2) during this same period was enough to overwhelm the small daytime uptake rate and result in a net loss of carbon. All other years demonstrated a negative NEE during the ablation period, indicating net carbon uptake, with the greatest in magnitude being -92.02 gC/m^2 occurring in 2007; a year with an ablation period average temperature of 5.0°C and the maximum peak SWE magnitude (454.7 mm) for the period of record.

There was a significant negative correlation between total ablation period carbon uptake (dependent variable) and ablation period mean air temperature and peak SWE magnitude (independent variables; $R^2=0.79$, $P<0.001$) that produced the following multiple linear regression equation:

$$(2) \quad NEE = 54.956 - (5.4992 * T) - (222.9 * SWE)$$

where NEE is the total ablation period NEE (gC/m^2), T is the ablation-period mean air temperature ($^\circ\text{C}$) and SWE is peak SWE (m). The range in the observed NEE that was fit with

equation (2) demonstrates that early season NEE is strongly coupled with snowpack dynamics. We note that ablation period mean air temperature and peak SWE magnitude did not exhibit collinearity for the observed record (Variable Inflation Factor=1.09) and that SWE had a greater influence than temperature in predicting total ablation period NEE. We use equation (2) to demonstrate potential current and future scenarios of ablation period NEE under various temperature-SWE magnitude scenarios. Fig. 3 displays the range of model results overlaid with the observed data. For an example future scenario corresponding to mid-century Western US projected SWE reductions of 20% percent [Leung *et al.*, 2004] and snowmelt timing shift of two weeks earlier [Stewart *et al.*, 2004; Clow, 2010], the mean ablation period NEE is predicted to decline by approximately 45% compared with the observed record.

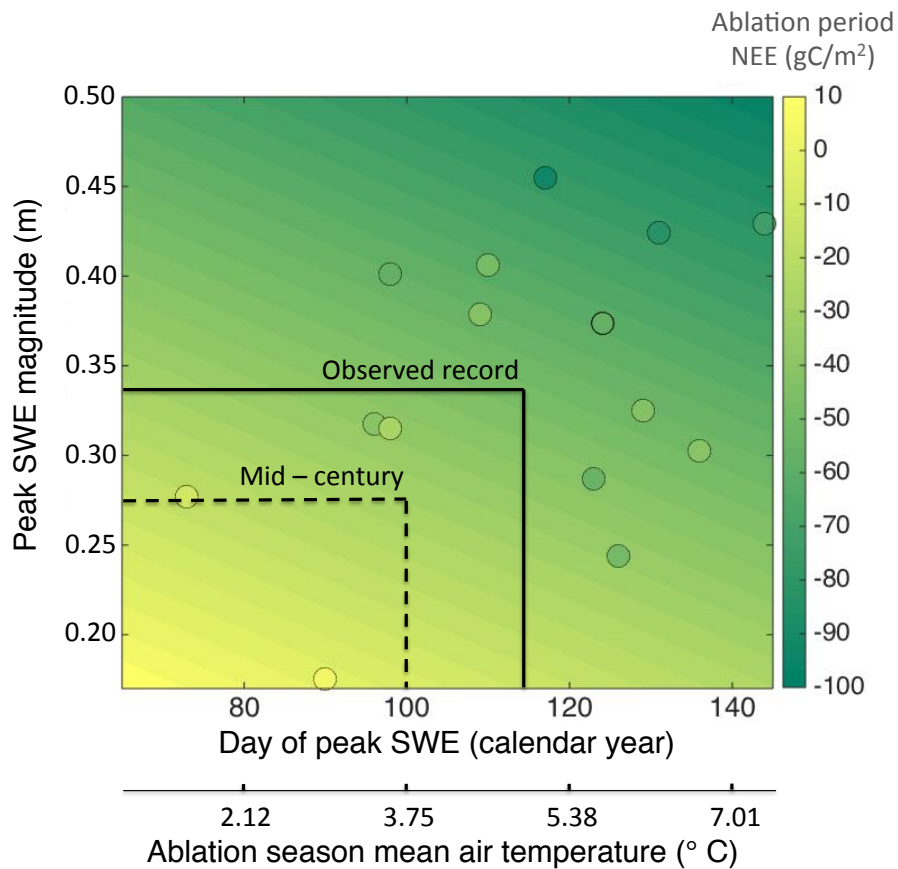


Figure 3 | Model output results from equations (1) and (2) demonstrating the range of potential ablation period total NEE. Each scatter point is an ablation period from the observed record. The solid lines represent the mean day of peak SWE and peak SWE magnitude from the observed record and the dotted lines represent the projected mid-century scenario.

In Fig. 4, we analyzed the contribution of the ablation period NEE to the full-season NEE (cumulative NEE from the date of peak SWE to the end of the previously defined non-ablation period). Fig. 4a shows a significant positive correlation ($R^2=0.42$, $P<0.01$) between the ratio of ablation period NEE to full-season NEE and the date of peak SWE, indicating that when peak SWE occurred later in the year, the relative uptake contribution of the ablation period increased. Two years (2007 & 2013) had a ratio of approximately 0.31, demonstrating that the ablation period NEE can comprise >30% of full-season NEE. However, as the date of peak SWE shifted to earlier in the year, the relative uptake contribution from the ablation period approached zero. Therefore, as the ablation period continues to shift earlier in the year under climate warming, the resulting seasonal net carbon uptake will be more dependent upon the dynamics of the non-ablation period. Fig. 4b shows there was no significant relationship between the ratios of ablation NEE/full-season NEE and ablation period length/full-season length; therefore, seasons with a relatively high ratio of ablation period NEE/full-season NEE can occur during years in which the ablation period length constitutes either a high or a low proportion of the full-season length. Finally, we note that we did not find a significant relationship between date of peak SWE and full-season NEE ($R^2=0.06$, $P=0.39$, supplemental Fig. A2 – Appendix A).

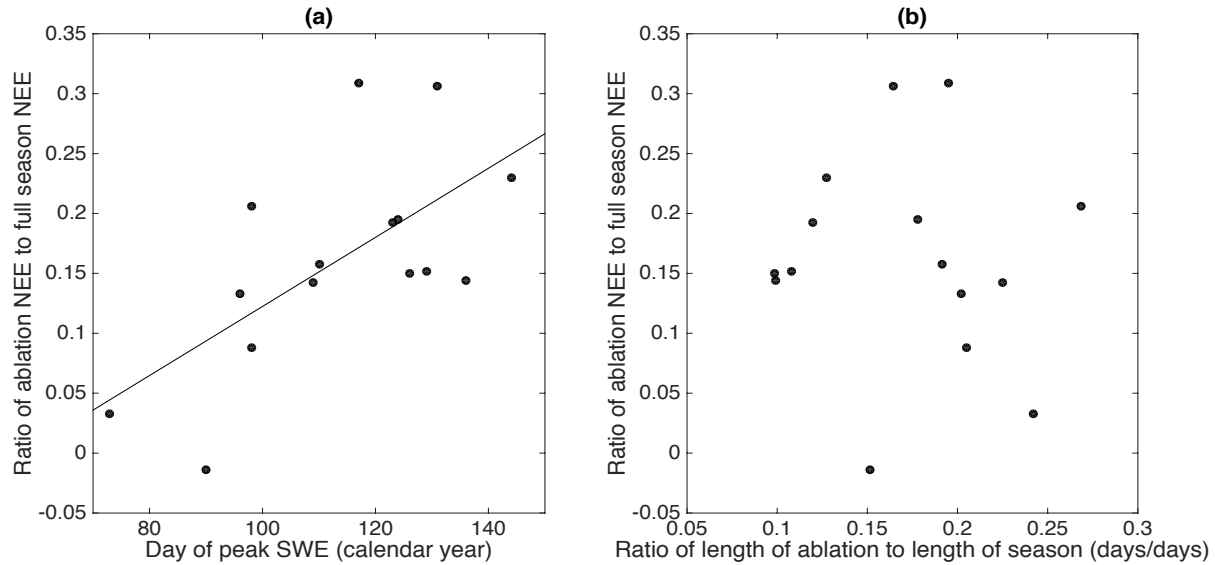


Figure 4 | (a) Relationship between the date of peak SWE (horizontal axis) and the ratio of ablation period NEE to full-season NEE (vertical axis) ($R^2=0.42$, $P<0.01$). (b) Relationship between the ratio of the length of the ablation season to length of the full season (horizontal axis) and the ratio of ablation period NEE to full-season NEE (vertical axis).

Discussion

In the 21st century the Rocky Mountain region is projected to experience a 2.0-3.5°C temperature increase in mean-annual temperatures relative to the end of the 20th century [Baldwin *et al.*, 2003]. By the nature of the precipitation phase dependence on temperature, warming has vast implications for snowpack accumulation and melting patterns. For example, snow melts earlier under warming scenarios [Stewart *et al.*, 2004; Clow, 2010] due to increases in incident thermal radiation and sensible heat flux. Additionally, warmer air temperatures reduce snowpack cooling in the winter period, which, in addition to reduced SWE accumulation, reduces the energy required to bring the snowpack to 0°C and initiate snowmelt. The influence of warming on ablation timing can be exacerbated by the effects of decreased snowpack albedo brought about by snowpack dust loading [Painter *et al.*, 2012].

Our results indicate that the timing of snowmelt determines the alignment of the ablation period with the seasonal temperature cycle, whereby early melt occurs during colder periods of the seasonal temperature cycle. The magnitudes of ablation period daily NEE rates were shown to decrease under colder temperature conditions. Thus, as ablation shifts earlier under climate warming and aligns with the colder periods of the seasonal temperature cycle, ablation period NEE trends to decrease. This concept presents a notable paradox: as global temperatures slowly rise, mid-latitude subalpine forests are likely to experience colder temperatures during the ablation season as a result of the shift in snowmelt timing with respect to the seasonal air temperature cycle. Therefore, warming temperatures will likely lead to less CO₂ uptake during the annual ablation period. Additionally, it is predicted that future warming will cause a larger fraction of winter precipitation to fall as rain, rather than snow [Scott-Denton *et al.*, 2013]. This phenomenon is a contributing factor in decreasing SWE magnitude. Declines in peak SWE will further contribute to a decreasing trend in ablation period carbon uptake.

It is perhaps surprising that we did not observe a significant relationship between daily NEE and PPFD. Importantly, the results of this study demonstrate that ablation period air temperature has a much stronger seasonal-phenological influence on ablation period daily NEE compared with PPFD. Additionally, we note that this ablation period temperature influence acts primarily on the process of forest carbon uptake, as we observed a substantially greater range in daytime NEE (when photosynthesis is actively occurring) opposed to nighttime NEE when respiration is the dominant process. Regarding the greater influence of SWE compared with air temperature in predicting total ablation period NEE, we suggest that this may be a result of varying ablation period lengths and/or a limitation of the 15-year length of the dataset. We find it

imperative to emphasize that, as shown in Fig. 2b, air temperature strongly influences daily NEE during the ablation period, which contributes a deeper understanding of forest phenological processes during the ablation period. In predicting total ablation period NEE, temperature and SWE magnitude are both important and allow us to generate future ablation period NEE scenarios, thus contributing to our understanding of carbon uptake trends under a warming scenario in seasonally snow-covered environments.

Our analysis used gap-filled data to develop the best estimate of cumulative NEE during the ablation period. The specific gap-filling technique was based on a model that uses net radiation, temperature and wind speed to produce half-hourly NEE values. The median percentage of model gap-filled data per ablation period was 8.13%. There were three years that had gap-filled percentages greater than 20% (2003–21%; 2006–35%; 2009–35%). If we remove these three high gap fraction years from our analysis, the relationships were rather unaffected, implying that these higher percentage gap-filled years were not having undue influence on the results. The coefficient of determination of the date of peak SWE vs. ablation-period mean air temperature relationship decreased only slightly from $R^2=0.72$ for all years to $R^2=0.70$ when excluding the three high gap fraction years. Additionally, the coefficient of determination of the ablation-period mean air temperature vs. daily NEE decreased only slightly from $R^2=0.87$ for all years to $R^2=0.86$ when excluding the three high gap fraction years.

In developing a complete understanding of the annual carbon budget it is important to also consider the NEE trends during the times preceding and following the ablation period. It has been demonstrated that shallower winter snowpacks result in colder soil temperatures and thus less soil respiration during the snow cover period (accumulation+ablation) [Monson *et al.*, 2006].

This reduction in wintertime respiration (less carbon release) acts in opposition to the potential reduction in ablation period carbon uptake proposed in this study. The fact that ablation-period NEE, which represents the sum of opposing photosynthesis and respiration CO₂ fluxes, decreases in seasons with earlier and colder snowmelt, is consistent with the conclusion that lower temperatures during snowmelt inhibits photosynthesis to a greater degree than respiration.

While we have a firm understanding as to how the NEE trends will progress during the periods of snow accumulation and snowmelt under changing snowpack dynamics, it is less clear as to how the respiration-uptake balance during the snow-free period will respond as future trends in summer precipitation and soil water availability are uncertain. The reported lack of correlation between the date of peak SWE and full-season NEE indicates that there is a decoupling in NEE processes between the ablation period and snow-free period. Thus, future work should focus on analyzing the factors that control NEE processes during the non-ablation period of the growing season. That said, isotopic signatures of xylem water suggest that snowmelt, as opposed to summer rainfall, is the primary driver of forest water availability [*Hu et al.*, 2010]. Hence, the ablation-period NEE climate sensitivities reported here have important implications for developing robust predictions of future terrestrial carbon cycling in seasonally snow-covered forests.

Conclusion

Using 15 years of SWE and eddy-covariance CO₂ measurements in Colorado we showed that temperature is a strong phenological control on ablation period daily NEE. Early ablation periods shifted melt to colder periods of the seasonal air temperature cycle, which resulted in lower magnitude daily NEE because of the strong phenological temperature influence on

ablation period NEE. These results represent an important paradox whereby climate warming shifts the timing of snowmelt to colder periods of the seasonal temperature cycle, which acts to decrease NEE. Projecting forward our multilinear-regression model to predict future ablation period NEE scenarios, a 45% reduction in mid-century ablation-period NEE is estimated. In building our understanding of NEE processes during the growing season as a whole, it is important that we first develop a firm grasp on NEE processes during the two distinct periods that together compose the growing season (snow ablation period+snow free period). This study provides evidence that snowpack dynamics are a strong control on forest carbon uptake during the snow ablation period. Future efforts should be directed toward an improved understanding of NEE processes during the snow-free period of the growing season, with a focus on how future precipitation and temperature scenarios will affect the balance between photosynthetic carbon uptake and ecosystem respiration.

Chapter II: Global Variation of the Rain Snow Temperature Threshold

Introduction

Precipitation phase partitioning determines both the timing and quantity of streamflow, with a shift from snow toward rain leading toward a decrease in streamflow volume and earlier streamflow timing [Barnett *et al.*, 2005; Berghuijs *et al.*, 2014]. This phase-streamflow relationship has important implications for water resources management as more than one-sixth of the global population is dependent on glaciers and seasonal snow packs as a water supply [Barnett *et al.*, 2005]. Recent trends in the western US have demonstrated that winter climate warming has contributed toward decreased SWE accumulation [Mote, 2003, 2006; Knowles *et al.*, 2006], which has subsequently resulted in earlier melt with slower snowmelt rates [Trujillo and Molotch, 2014] and less annual streamflow [Barnhart *et al.*, 2016]. As we expect this trend to continue, with a still greater proportion of future precipitation predicted to fall as rain, rather than snow [Scott-Denton *et al.*, 2013], it becomes increasingly important to improve phase-partitioning schemes so that we can continually improve the accuracy of hydrologic forecasts under progressively stressful water resources conditions.

Auer [1974] demonstrated that there is a near-surface air temperature-precipitation phase relationship and that snow can occur at temperatures much greater than 0°C. Feiccabrino and Lundberg [2008], Fassnacht *et al.* [2013] and Kienzle [2008] have subsequently developed additional, region specific, phase partitioning schemes based only on near-surface air temperature. Phase-partitioning methods that are based on simple empirical relationships with near-surface air temperature, however, ignore additional physically relevant variables (i.e. relative humidity, surface pressure) that could produce a phase distinction between two

precipitation events that occur at the same air temperature. Most current precipitation-phase partitioning methods represent a large source of uncertainty for hydrologic models that can be improved with the inclusion of additional physical variables [*Harder and Pomeroy, 2014*].

In this study we used a 29-year global observational dataset to explore the influence of surface air temperature, relative humidity and surface pressure on precipitation phase. These three variables are of particular importance with regards to precipitation phase due to their influence on the energy balance of a hydrometeor. From an energy balance perspective, precipitation that falls through a dry ambient atmosphere (low relative humidity) loses heat through evaporative cooling as it is falling. Therefore, if a snow crystal forms in the cold ($T < 0^{\circ}\text{C}$) upper atmosphere and falls through a warm ($T > 0^{\circ}\text{C}$) lower atmosphere, the snow crystal is less likely to be melted by the atmospheric sensible heat input if the relative humidity is low and the crystal experiences evaporative cooling. As the relative humidity approaches 100%, the crystal experiences less evaporative cooling and is more likely to fall as rain in the warm ambient atmosphere. Regarding pressure, hydrometeors that fall through areas of lower surface pressure experience less drag force and thus theoretically can fall faster, spending less time in the warm ambient atmosphere, than if falling through areas of higher surface pressure. In this study we explore the global influence of air temperature, relative humidity and surface pressure in order to further develop our understanding of precipitation phase patterns in varying land surface conditions. Froidurot et al. [2014] and Ding et al. [2014] have conducted studies which evaluate the precipitation phase influence of relative humidity and elevation (proxy for surface pressure); however, these studies are region specific and thus limited in both the spatial extent and quantity of data. Our study provides the most extensive empirical evaluation to date of the influence of air temperature, relative humidity and surface pressure on precipitation phase.

We note that this study builds upon the work of Dai [2008]. Dai used the same 29-year observational dataset to develop conditional snow frequency curves for both the land and the ocean. We extend Dai's study by further exploring various physical variables that may influence conditional snow frequency curves throughout the land surface, specifically addressing how low relative humidity and/or reduced surface pressure may enable snow to fall at greater frequencies at higher surface air temperatures relative to precipitation events falling at high relative humidity and/or high surface pressure.

Data and Methods

a) Dataset and Station Data Analysis

We used the NCEP ADP Operational Global Surface Observations dataset (DS464.0) that is hosted by the National Center for Atmospheric Research (<http://rda.ucar.edu/datasets/ds464.0/>). This dataset includes 6 and 3-hourly synoptic weather reports that include air temperature (T_s), dew point temperature (T_d), surface pressure (P_s) and precipitation phase (measurements collected at ~ 1.5 - 2.0 m above ground). Observational station data records were sourced from both land and ocean stations. In this study we used data exclusively from land stations, however, some stations are in regions where precipitation falls exclusively as rain and thus by default were not included in this study. Fig. 1 displays the regional distribution of the stations that contributed data to our study (12,276 stations). Dai [2008] used this same dataset for his study of 50% snow frequency surface temperatures over land and ocean. We used the same precipitation phase distinctions described in detail in Dai [2008] to determine whether a precipitation event fell as rain, snow or sleet. Ambient relative humidity (RH) was calculated per precipitation event according to the same methods used by Dai

[2006]. For quality control purposes, we removed precipitation events from the dataset that had a calculated relative humidity of less than 10% or greater than 100%.

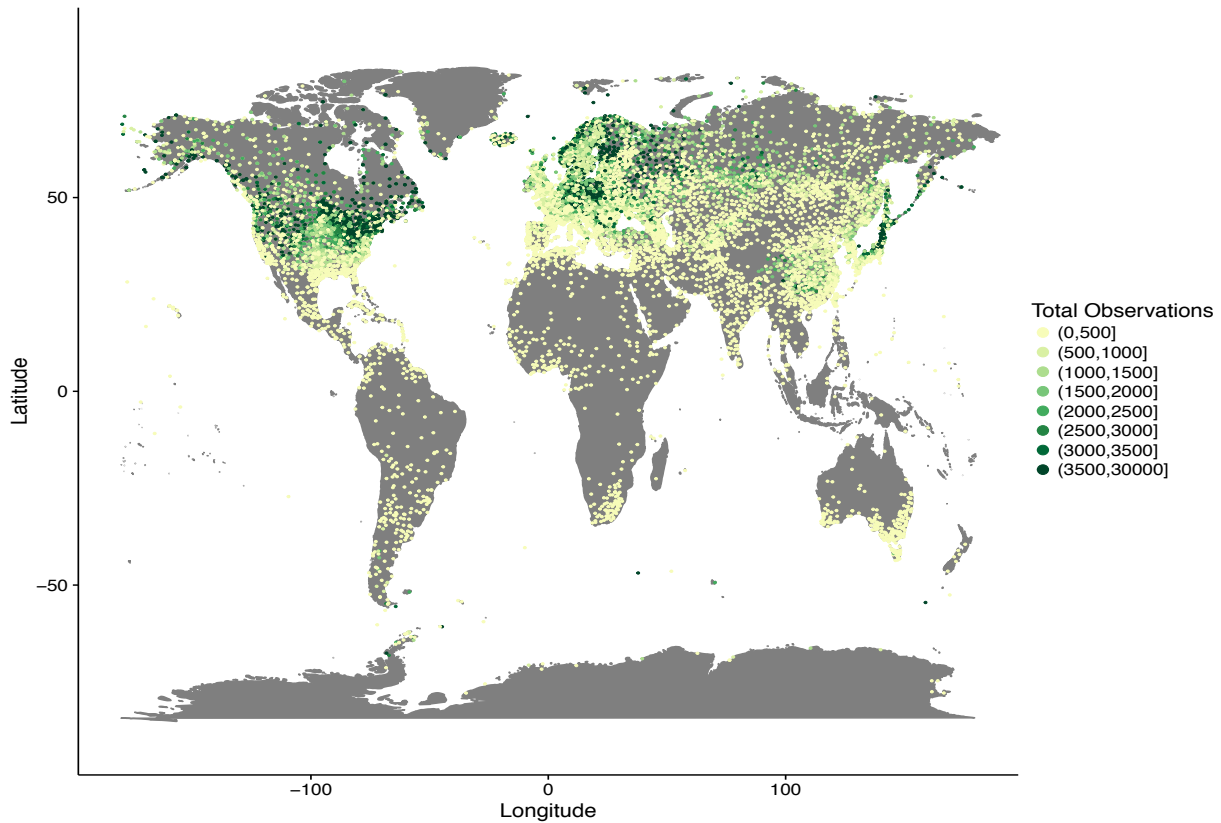


Figure 1 | Global distribution of stations from the DS464.0 dataset that contributed data to our study (12,276 stations). The median number of observations per station was 460. The maximum number of observations contributed by a single station was 28,882 and the minimum number of observations contributed by a single station was 1. The color bins increase by increments of 500 observations until the final bin, which increments from 3,500 to 30,000 observations.

We focused our station data analysis on precipitation events that fell between $-0.5\text{ }^{\circ}\text{C}$ and $5.5\text{ }^{\circ}\text{C}$, typically the range in which precipitation events fall as either snow, rain, or sleet (below $-0.5\text{ }^{\circ}\text{C}$ the majority of events occur as snow and above $5.5\text{ }^{\circ}\text{C}$ the majority of events occur as rain). We binned all events into 1-degree temperature bins ($-0.5\text{-}0.5\text{ }^{\circ}\text{C}$, $0.5\text{-}1.5\text{ }^{\circ}\text{C}$, $1.5\text{-}2.5\text{ }^{\circ}\text{C}$, $2.5\text{-}3.5\text{ }^{\circ}\text{C}$, $3.5\text{-}4.5\text{ }^{\circ}\text{C}$, $4.5\text{-}5.5\text{ }^{\circ}\text{C}$) for the phase frequency analysis, which included a separate analysis of six relative humidity classes (40-50%, 50-60%, 60-70%, 70-80%, 80-90%, 90-100%)

and four pressure classes (60-70 kPa, 70-80 kPa, 80-90 kPa, 90-105 kPa). After filtering the dataset for the station data analysis, there were 12,832,163 precipitation observations that occurred within the stated temperature range, humidity range and pressure range. Table 1 and Table 2 display the total number of observations per relative humidity class and per pressure class, respectively. For each precipitation observation, we used the recorded Ts, Td and Ps to calculate the ambient RH during the event observation interval. We note that many stations did not record Ps but do maintain records of Ts, Td and precipitation phase. When this was the case, to calculate RH for the observation we used the 1978-2007 average wintertime (December-January-February) Ps from the MERRA reanalysis dataset for the grid cell in which the station observation was located. For the stations that do record Ps, we find that the MERRA reanalysis Ps data closely matches the station Ps observations (mean percent difference = 0.11%).

	Relative Humidity Class					
	40-50%	50-60%	60-70%	70-80%	80-90%	90-100%
Total Observations	38,786	148,796	406,094	863,244	3,163,547	8,211,696

Table 1 | Total number of precipitation observations between -0.5 °C and 5.5 °C per 10% relative humidity class

	Pressure Class			
	60-70 kPa	70-80 kPa	80-90 kPa	90-105 kPa
Total Observations	52,940	168,236	892,116	11,718,871

Table 2 | Total number of precipitation observations between -0.5 °C and 5.5 °C per pressure class

b) Model

Similar to Froidurot et al. [2014], we performed an empirical binary logistic regression model analysis using Ts, RH and Ps as predictor variables for precipitation phase. Our model development methods similarly compared to Froidurot et al. [2014] in the following ways: 1) Both study model sets predicted the probability of rain; 2) Both study model sets use data in the temperature range of greater than -3 °C to less than 5 °C (note that for the model analysis we alter the temperature range from our station data analysis); 3) Sleet data is removed from both study datasets in the model analysis. The primary reason for removing sleet data from the model analysis is the limitation by which the dataset does not report the proportion of solid and liquid precipitation for mixed events. The minimal impact of removing sleet data from the model analysis is detailed in Froidurot et al. [2014]; and 4) for both study model sets, if the model predicted that the probability of rain was greater than 50%, the event was deemed to be a rain event. The main difference between our set of models and the set produced in the Froidurot et al. [2014] study was the size and the spatial extent of the datasets. The Froidurot et al. dataset had 68,434 data points that were exclusively from Switzerland. The NCEP DS464.0 dataset used for the model analysis in this study had 14,900,606 observations ranging throughout the globe (primarily in the northern hemisphere), approximately 218 times more observations than the Froidurot et al. dataset. We note that the temperature range we analyzed in the models is greater than the temperature range explored in the station data analysis and thus resulted in more data points used in the model analysis compared with the station data analysis. Note that we included sleet data in our station data analysis, but removed it from the modeling analysis per the reasons set forth by Froidurot et al. [2014]. The median elevation of the stations contributing observations to the NCEP DS464.0 dataset was 157 m.

For comparison of the impact of the three predictor variables, we developed three different empirical binary logistic regression models:

Temperature only model (Ts):

$$(1) \quad p(rain) = \frac{1}{1 + e^{(\alpha + \beta * Ts)}}$$

Temperature and relative humidity model (Ts-RH):

$$(2) \quad p(rain) = \frac{1}{1 + e^{(\alpha + \beta * Ts + \gamma * RH)}}$$

Temperature, relative humidity and pressure model (Ts-RH-Ps):

$$(3) \quad p(rain) = \frac{1}{1 + e^{(\alpha + \beta * Ts + \gamma * RH + \lambda * Ps)}}$$

where α , β , γ , λ are model coefficients. We utilized an empirical modeling scheme, as opposed to an analytical scheme, due to the spatial and temporal variability, scarcity, and errors inherent in the dataset, as well as a lack of physical information regarding the conditions in the atmospheric column above ~1.5-2 m. To obtain the model coefficients, we ran 250 training simulations with each simulation using 5000 randomly selected global observations to develop simulation coefficients. For each of the three models, we took the mean of the 250 sets of training coefficients to obtain the final model coefficients. To test the three resulting models, we

removed the training observations from the dataset and split the remaining validation dataset into 10% relative humidity classes (40-50%, 50-60%, 60-70%, 70-80%, 80-90%, 90-100%) and tested the success rate of each model in predicting global precipitation events within each relative humidity class. This allowed us to compare how each model performed at predicting events in varying relative humidity classes.

Results

a) Station Data Relative Humidity

The six panels of fig. 1 display the precipitation phase frequencies at the given air temperatures for each of the six relative humidity classes. Each panel contains every precipitation event in the 29-year record that fell within the 10% relative humidity bin reported at the top of the panel. We observed that precipitation events that fell at a low relative humidity are more likely to fall as snow at higher temperatures. In the 40-50% relative humidity bin, for example, the snow frequency at 5°C was 57.4%. In contrast, in the 90-100% relative humidity bin, the snow frequency dropped close to 0% at 2°C. Fig. 2 isolates the snow frequency curves per relative humidity bin onto the same plot. We observed that at 0°C all snow frequency values are greater than 75%. As the temperature increased, however, the curves undergo a stark separation with the snow frequency of the higher relative humidity curves dropping quickly toward zero, whereas the lower relative humidity curves maintain greater snow frequency values at higher temperatures. We note that the total number of observations was substantially less for the low RH bins compared with the high RH bins, with the significant majority of observations having occurred in the 90-100% RH bin.

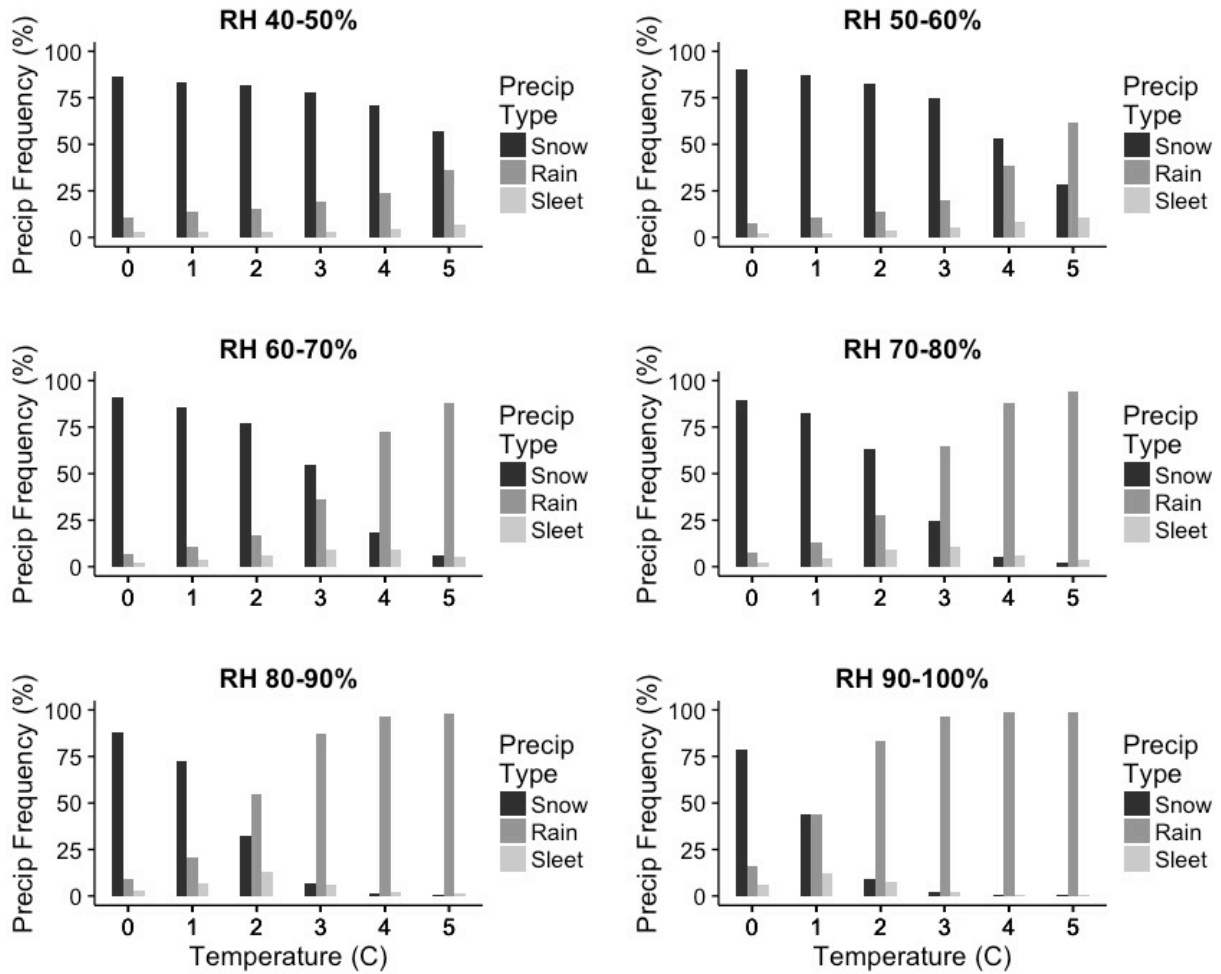


Figure 2 | Precipitation frequency plots for varying ranges of relative humidity. Each panel contains all precipitation events that fell within the labeled relative humidity bin at the plotted temperatures. Contained within these six panels are 12,832,163 precipitation observations. Temperature observations were collected at ~1.5-2m above ground.

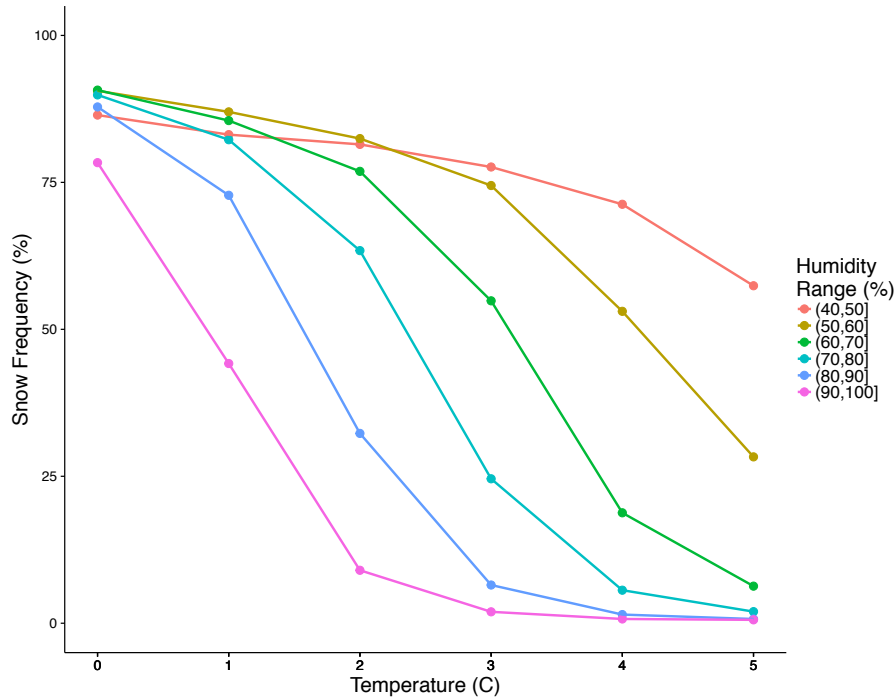


Figure 3 | Observational snow frequency percentages per relative humidity class. At 0°C, the snow frequencies rank as follows, with the corresponding humidity range in parenthesis: 90.7% (60-70%), 90.6% (50-60%), 89.9% (70-80%), 87.8% (80-90%), 86.5% (40-50%), 78.4% (90-100%).

b) Station Data Pressure

The four panels of fig. 3 display the precipitation phase frequencies at the given air temperatures for each of the four pressure classes. Similar to the layout of fig. 1, each panel contains every precipitation event in the 29-year record that fell within the pressure bin reported at the top of the panel. At the higher temperatures we observed higher snow frequencies in the lower pressure bins. However, the range of snow frequency values at the higher temperatures was not as great compared with the relative humidity binned snow frequency range at the higher temperatures. Fig. 4 isolates the snow frequency curves per pressure bin onto the same plot. At the higher temperatures we observed the highest snow frequency values at lower pressures. However, as mentioned, comparisons of fig. 3 and fig. 5 demonstrates that the range in snow

frequency values between Ps bins was not as great at the higher temperatures when compared with the RH bins. Again, we note that table 2 demonstrates that the number of observations was substantially less for the low Ps bins compared with the high Ps bins, with the significant majority of observations having occurred in the 90-105 kPa bin.

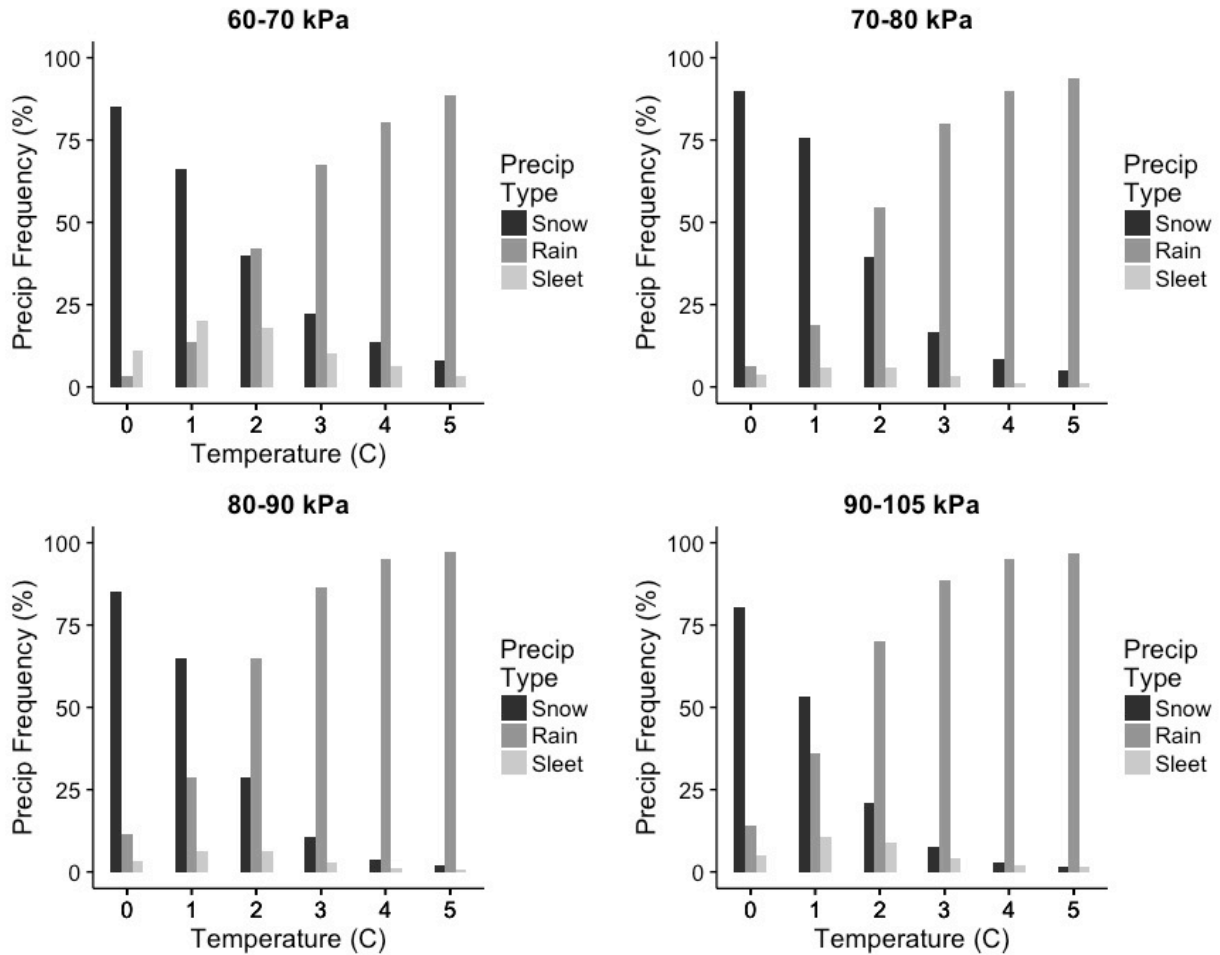


Figure 4 | Precipitation frequency plots for varying ranges of surface pressure. Each panel contains all precipitation events that fell within the labeled surface pressure bin at the plotted temperatures. Contained within these four panels are 12,832,163 precipitation observations. Temperature observations were collected at ~1.5-2m above ground.

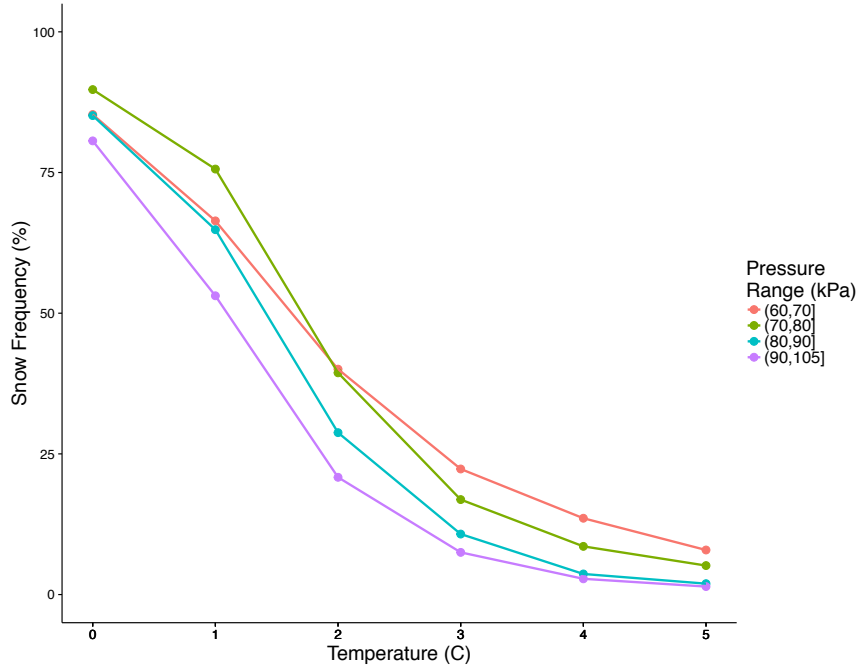


Figure 5 | Observational snow frequency percentages per surface pressure class. At 0°C, the snow frequencies rank as follows, with the corresponding pressure range in parenthesis: 89.7% (70-80), 85.3% (60-70 kPa), 85.1% (80-90 kPa), 80.6% (90-100 kPa).

c) Model Analysis

Table 3 presents the coefficients calibrated for each of the three models (Ts, Ts-RH, Ts-RH-Ps). Table 4 displays the success rate of each model in predicting the precipitation phase of the validation data within each RH bin. We observed that the Ts-RH and Ts-RH-Ps models produced similar success rates for each RH bin. The Ts-RH and Ts-RH-Ps models were more successful than the Ts model for each RH bin; however, the difference in success rates between these models decreased with increases in RH. For example, the Ts-RH model was 26.8% more successful than the Ts model at the 40-50% RH class and only 1.4% greater at the 90-100% RH class. Overall, the success rates for each model tended to increase with increases in the RH bin. All models had maximum success rates between 88-89%.

Model	α	β (Ts)	γ (RH)	λ (Ps)
Ts (eqn. 1)	-1.54 (0.06)	1.24 (0.04)	-	-
Ts-RH (eqn. 2)	-10.04 (0.68)	1.41 (0.05)	0.09 (0.007)	-
Ts-RH-Ps (eqn. 3)	-12.80 (1.07)	1.41 (0.05)	0.09(0.007)	0.03 (0.008)

Table 3 | Coefficients for the Ts, Ts-RH, and Ts-RH-Ps models with the coefficient standard deviations in parenthesis. Coefficients align with the binary logistic regression equations presented in the methods (eqns. (1), (2) and (3)), which predict the probability of rain as functions of varying combinations of Ts ($^{\circ}$ C), RH (%) and Ps (kPa)

	Relative Humidity Class					
	40-50%	50-60%	60-70%	70-80%	80-90%	90-100%
Total test observations	40,871	161,513	437,011	1,070,000	3,291,606	8,682,418
Ts Model Success (%)	51.5	60.1	72.3	83.8	88.0	86.7
Ts-RH Model Success (%)	78.3	80.5	83.5	88.7	88.6	88.1
Ts-RH-Ps Model Success (%)	77.6	80.5	83.6	88.7	88.7	88.1

Table 4 | Model success rates per relative humidity class

Discussion

As warming winter temperatures lead to decreased SWE accumulation [Mote, 2003, 2006; Knowles *et al.*, 2006] and subsequently stressed seasonal water supplies, it has become increasingly important to develop improved global modeling techniques to better understand and predict precipitation phase. Our study took a combined approach of 1) observationally analyzing a global hydrometeorological dataset to better understand how various physical variables allow precipitation to preferentially fall as snow at higher temperatures (station data analysis), and 2)

using the results of the station data analysis to develop the most extensive global phase prediction model to date (model analysis).

Our station data analysis indicated that precipitation events were much more likely to fall as snow at higher T_s when the RH was lower. The lowest RH bin (40-50%) had a snow frequency of over 50% at 5°C, and we observed a successive drop-off of snow frequency values with increases in RH. The highest RH bins had effectively 0% of events occur as snow at 5°C. Fig. 3 displays the large range in snow frequency values at high temperatures for the various RH bins. First principles suggest that high snow frequencies at high temperatures for the low RH bins were a result of evaporative cooling that occurs as snow crystals fall through a low RH ambient atmosphere. This cooling effect allows the crystals to remain frozen even though the ambient temperature may be greater than 0°C. We note that our RH calculations represent the conditions at ~1.5-2m above ground.

Fig. 5 demonstrates that the range in snow frequency values for the Ps bins was not nearly as large as it was for the RH bins, indicating that RH has a greater influence on precipitation phase compared with pressure. However, although the range in snow frequency values is low, the lower Ps bins did demonstrate the highest snow frequency values at the higher temperatures. First principles indicate that the greater snow frequency values at higher temperatures for the low Ps bins was influenced by snow crystals being able to fall at faster speeds through lower pressure environments, thus reducing the duration of exposure to warm ambient atmospheric conditions.

The binary logistic regression model results demonstrate that the T_s -RH and T_s -RH-Ps models performed effectively equivalently, and that both of these models uniformly performed better than the simple T_s model. The equivalent performance of the T_s -RH and T_s -RH-Ps

models indicates that adding Ps to the model does not improve model performance. Table 3 demonstrates that the greatest utility from adding RH into the model occurred in predicting precipitation phase in the lower RH bins. For example, the difference in success rates for predicting precipitation phase in the 40-50% RH bin between the Ts and Ts-RH models was 26.8%, whereas the difference in success rates for the 90-100% bin was 1.4%, therefore indicating that the utility of including RH in the model is greatest for predicting events that occur at low ambient RH. Therefore, while our results demonstrate that RH should be included in precipitation phase predictive models whenever possible, we might expect RH to more significantly contribute to models developed for climatically dry regions.

The binary logistic regression models proposed in this study can be applied to improve snowpack development within hydrologic models. Due to the spatial extent of the data and demonstrated high success of the models, the models can be applied in regions where other phase precipitation models do not currently exist.

Conclusion

Using 29 years of global precipitation phase data, we have presented the most spatially extensive binary logistic regression phase prediction model. While previous studies have produced regional binary logistic regression models, our models have been tested with high success rates on a global scale and thus can be used in regions that do not presently have existing models. Our model analysis demonstrated that a Ts-RH model had universally higher predictions success rates than the simple Ts model, with the most significant differences having occurred for predicting events that occurred at lower RH (Ts-RH model was 26.1% more successful than the simple Ts model in predicting events in the lowest relative humidity class). Thus, when RH data

is available, the Ts-RH model should be utilized for increased phase prediction success. The Ts-RH-Ps model generally performed slightly better than the Ts-RH model, however, the difference in success rates between the two models was often less than 1%. This result aligns with our station data analysis that showed a large range in snow frequencies at higher temperatures for different RH class events and only a small range in snow frequencies at higher temperatures for different Ps class events. Future efforts should be directed toward an improved understanding of snow crystal energy balance dynamics throughout the entire atmospheric profile, with a focus on the effects of RH and temperature throughout the profile. Additionally, the effectiveness of the models proposed in this study should be tested in areas where more high elevation data are available.

References

- Auer, A.H. (1974), The rain versus snow threshold temperatures, *27*, 67.
- Baldwin, C., F. H. Wagner, and U. Lall (2003), Rocky Mountain/Great Basin regional climate-change assessment report for the US global change research program. *Water Resources. Utah State University Press, Logan*, 79-112.
- Barnett, T. P., J. C. Adam, and D. P. Lettenmaier (2005), Potential impacts of a warming climate on water availability in snow-dominated regions., *Nature*, *438*(7066), 303–9, doi:10.1038/nature04141.
- Barnhart, T. B., N. P. Molotch, B. Livneh, A. A. Harpold, J. F. Knowles, and D. Schneider (2016), Snowmelt Rate Dictates Streamflow, *Geophys. Res. Lett.*, doi:10.1002/2016GL069690.
- Berghuijs, W., R. Woods, and M. Hrachowitz (2014), A precipitation shift from snow towards rain leads to a decrease in streamflow, *Nat. Clim. Chang.*
- Bernhardt, E. S., and W. H. Schlesinger (2013), Schlesinger, W.H. and E.S. Bernhardt. 2013. Biogeochemistry: An analysis of global change. 3rd edition. Elsevier. 688pp.,
- Black, T. A., W. J. Chen, A. G. Barr, M. A. Arain, Z. Chen, Z. Nestic, E. H. Hogg, H. H. Neumann, and P. C. Yang (2000), Increased carbon sequestration by a boreal deciduous forest in years with a warm spring, *Geophys. Res. Lett.*, *27*(9), 1271–1274, doi:10.1029/1999GL011234.
- Bradley, R. S. (2004), Projected temperature changes along the American cordillera and the planned GCOS network, *Geophys. Res. Lett.*, *31*(16), L16210, doi:10.1029/2004GL020229.
- Burns, S. P., P. D. Blanken, A. A. Turnipseed, J. Hu, and R. K. Monson (2015), The influence of warm-season precipitation on the diel cycle of the surface energy balance and carbon dioxide at a Colorado subalpine forest site, *Biogeosciences*, *12*(23), 7349–7377, doi:10.5194/bg-12-7349-2015.
- Clow, D. W. (2010), Changes in the Timing of Snowmelt and Streamflow in Colorado: A Response to Recent Warming, *J. Clim.*, *23*(9), 2293–2306, doi:10.1175/2009JCLI2951.1.
- Dai, A. (2006), Recent climatology, variability, and trends in global surface humidity, *J. Clim.*, *19*(15), 3589–3606, doi:10.1175/JCLI3816.1.
- Dai, A. (2008), Temperature and pressure dependence of the rain-snow phase transition over land and ocean, *Geophys. Res. Lett.*, *35*(12), 1–7, doi:10.1029/2008GL033295.
- Ding, B., K. Yang, J. Qin, L. Wang, Y. Chen, and X. He (2014), The dependence of precipitation types on surface elevation and meteorological conditions and its parameterization, *J. Hydrol.*, *513*, 154–163, doi:10.1016/j.jhydrol.2014.03.038.
- Dunn, A. L., C. C. Barford, S. C. Wofsy, M. L. Goulden, and B. C. Daube (2007), A long-term record of carbon exchange in a boreal black spruce forest: means, responses to interannual variability, and decadal trends, *Glob. Chang. Biol.*, *13*(3), 577–590, doi:10.1111/j.1365-2486.2006.01221.x.
- Fassnacht, S. R., N. B. H. Venable, J. Khishigbayar, and M. L. Cherry (n.d.), The probability of precipitation as snow derived from daily air temperature for high elevation areas of Colorado, United States, *IAHS-AISH Publ.*, 65–70.
- Feiccabrino, J., and A. Lundberg (2008), Precipitation Phase Discrimination in Sweden, *65th East. SNOW Conf.*, 239–254, doi:ISBN 0-920081-30-4 ISSN: 0424-1932.
- Flanner, M. G., K. M. Shell, M. Barlage, D. K. Perovich, and M. A. Tschudi (2011), Radiative

- forcing and albedo feedback from the Northern Hemisphere cryosphere between 1979 and 2008, *Nat. Geosci.*, 4(3), 151–155, doi:10.1038/ngeo1062.
- Froidurot, S., I. Zin, B. Hingray, and A. Gautheron (2014), Sensitivity of Precipitation Phase over the Swiss Alps to Different Meteorological Variables, *J. Hydrometeorol.*, 15(2), 685–696, doi:10.1175/JHM-D-13-073.1.
- Goulden, M. L. (1998), Sensitivity of Boreal Forest Carbon Balance to Soil Thaw, *Science* (80-.), 279(5348), 214–217, doi:10.1126/science.279.5348.214.
- Hamlet, A. F., P. W. Mote, M. P. Clark, and D. P. Lettenmaier (2005), Effects of Temperature and Precipitation Variability on Snowpack Trends in the Western United States*, *J. Clim.*, 18(21), 4545–4561, doi:10.1175/JCLI3538.1.
- Harder, P., and J. W. Pomeroy (2014), Hydrological model uncertainty due to precipitation-phase partitioning methods, *Hydrol. Process.*, 28(14), 4311–4327, doi:10.1002/hyp.10214.
- Harpold, A. A., and N. P. Molotch (2015), Sensitivity of soil water availability to changing snowmelt timing in the western U.S., *Geophys. Res. Lett.*, 42(19), 8011–8020, doi:10.1002/2015GL065855.
- Hu, J., D. J. P. Moore, S. P. Burns, and R. K. Monson (2010), Longer growing seasons lead to less carbon sequestration by a subalpine forest, *Glob. Chang. Biol.*, 16(2), 771–783, doi:10.1111/j.1365-2486.2009.01967.x.
- Huxman, T. E., A. A. Turnipseed, J. P. Sparks, P. C. Harley, and R. K. Monson (2003), Temperature as a control over ecosystem CO₂ fluxes in a high-elevation, subalpine forest., *Oecologia*, 134(4), 537–46, doi:10.1007/s00442-002-1131-1.
- Kienzle, S. W. (2008), A new temperature based method to separate rain and snow, *Hydrol. Process.*, 22(26), 5067–5085, doi:10.1002/hyp.7131.
- Knowles, N., M. D. Dettinger, D. R. Cayan, N. Knowles, M. D. Dettinger, and D. R. Cayan (2006), Trends in Snowfall versus Rainfall in the Western United States, <http://dx.doi.org/10.1175/JCLI3850.1>.
- Leung, L. R., Y. Qian, X. Bian, W. M. Washington, J. Han, and J. O. Roads (2004), Mid-Century Ensemble Regional Climate Change Scenarios for the Western United States, *Clim. Change*, 62(1-3), 75–113, doi:10.1023/B:CLIM.0000013692.50640.55.
- Mitchell, S. R., R. E. Emanuel, and B. L. McGlynn (2015), Land–atmosphere carbon and water flux relationships to vapor pressure deficit, soil moisture, and stream flow, *Agric. For. Meteorol.*, 208, 108–117, doi:10.1016/j.agrformet.2015.04.003.
- Monson, R. K., A. A. Turnipseed, J. P. Sparks, P. C. Harley, L. E. Scott-Denton, K. Sparks, and T. E. Huxman (2002), Carbon sequestration in a high-elevation, subalpine forest, *Glob. Chang. Biol.*, 8(5), 459–478, doi:10.1046/j.1365-2486.2002.00480.x.
- Monson, R. K., J. P. Sparks, T. N. Rosenstiel, L. E. Scott-Denton, T. E. Huxman, P. C. Harley, A. A. Turnipseed, S. P. Burns, B. Backlund, and J. Hu (2005), Climatic influences on net ecosystem CO₂ exchange during the transition from wintertime carbon source to springtime carbon sink in a high-elevation, subalpine forest., *Oecologia*, 146(1), 130–47, doi:10.1007/s00442-005-0169-2.
- Monson, R. K., D. L. Lipson, S. P. Burns, A. A. Turnipseed, A. C. Delany, M. W. Williams, and S. K. Schmidt (2006), Winter forest soil respiration controlled by climate and microbial community composition., *Nature*, 439(7077), 711–4, doi:10.1038/nature04555.
- Mote, P. W. (2003), Trends in snow water equivalent in the Pacific Northwest and their climatic causes, *Geophys. Res. Lett.*, 30(12), doi:10.1029/2003GL017258.

- Mote, P. W. (2006), Climate-Driven Variability and Trends in Mountain Snowpack in Western North America*, *J. Clim.*, 19(23), 6209–6220, doi:10.1175/JCLI3971.1.
- Nogués-Bravo, D., M. B. Araújo, M. P. Errea, and J. P. Martínez-Rica (2007), Exposure of global mountain systems to climate warming during the 21st Century, *Glob. Environ. Chang.*, 17(3-4), 420–428, doi:10.1016/j.gloenvcha.2006.11.007.
- Painter, T. H., S. M. Skiles, J. S. Deems, A. C. Bryant, and C. C. Landry (2012), Dust radiative forcing in snow of the Upper Colorado River Basin: 1. A 6 year record of energy balance, radiation, and dust concentrations, *Water Resour. Res.*, 48(7), n/a–n/a, doi:10.1029/2012WR011985.
- Pan, Y. et al. (2011), A large and persistent carbon sink in the world's forests., *Science*, 333(6045), 988–993, doi:10.1126/science.1201609.
- Piao, S. et al. (2008), Net carbon dioxide losses of northern ecosystems in response to autumn warming., *Nature*, 451(7174), 49–52, doi:10.1038/nature06444.
- Richardson, A. D. et al. (2010), Influence of spring and autumn phenological transitions on forest ecosystem productivity., *Philos. Trans. R. Soc. Lond. B. Biol. Sci.*, 365(1555), 3227–46, doi:10.1098/rstb.2010.0102.
- Sacks, W. J., D. S. Schimel, and R. K. Monson (2007), Coupling between carbon cycling and climate in a high-elevation, subalpine forest: a model-data fusion analysis., *Oecologia*, 151(1), 54–68, doi:10.1007/s00442-006-0565-2.
- Schimel, D., T. G. F. Kittel, S. Running, R. Monson, A. Turnipseed, and D. Anderson (2002), Carbon sequestration studied in western U.S. mountains, *Eos, Trans. Am. Geophys. Union*, 83(40), 445, doi:10.1029/2002EO000314.
- Scott-Denton, L. E., D. J. P. Moore, N. A. Rosenbloom, T. G. F. Kittel, S. P. Burns, D. S. Schimel, and R. K. Monson (2013), Forecasting net ecosystem CO₂ exchange in a subalpine forest using model data assimilation combined with simulated climate and weather generation, *J. Geophys. Res. Biogeosciences*, 118(2), 549–565, doi:10.1002/jgrg.20039.
- Stewart, I. T., D. R. Cayan, and M. D. Dettinger (2004), Changes in Snowmelt Runoff Timing in Western North America under a 'Business as Usual' Climate Change Scenario, *Clim. Change*, 62(1-3), 217–232, doi:10.1023/B:CLIM.0000013702.22656.e8.
- Stewart, I. T., D. R. Cayan, M. D. Dettinger, I. T. Stewart, D. R. Cayan, and M. D. Dettinger (2005), Changes toward Earlier Streamflow Timing across Western North America, <http://dx.doi.org/10.1175/JCLI3321.1>.
- Trujillo, E., and N. P. Molotch (2014), Snowpack regimes of the Western United States, *Water Resour. Res.*, 50(7), 5611–5623, doi:10.1002/2013WR014753.
- Turnipseed, A. A., P. D. Blanken, D. E. Anderson, and R. K. Monson (2002), Energy budget above a high-elevation subalpine forest in complex topography, *Agric. For. Meteorol.*, 110(3), 177–201, doi:10.1016/S0168-1923(01)00290-8.
- Turnipseed, A. A., D. E. Anderson, P. D. Blanken, W. M. Baugh, and R. K. Monson (2003), Airflows and turbulent flux measurements in mountainous terrain, *Agric. For. Meteorol.*, 119(1-2), 1–21, doi:10.1016/S0168-1923(03)00136-9.
- Wu, C. et al. (2013), Interannual variability of net ecosystem productivity in forests is explained by carbon flux phenology in autumn, *Glob. Ecol. Biogeogr.*, 22(8), 994–1006, doi:10.1111/geb.12044.

Appendix A

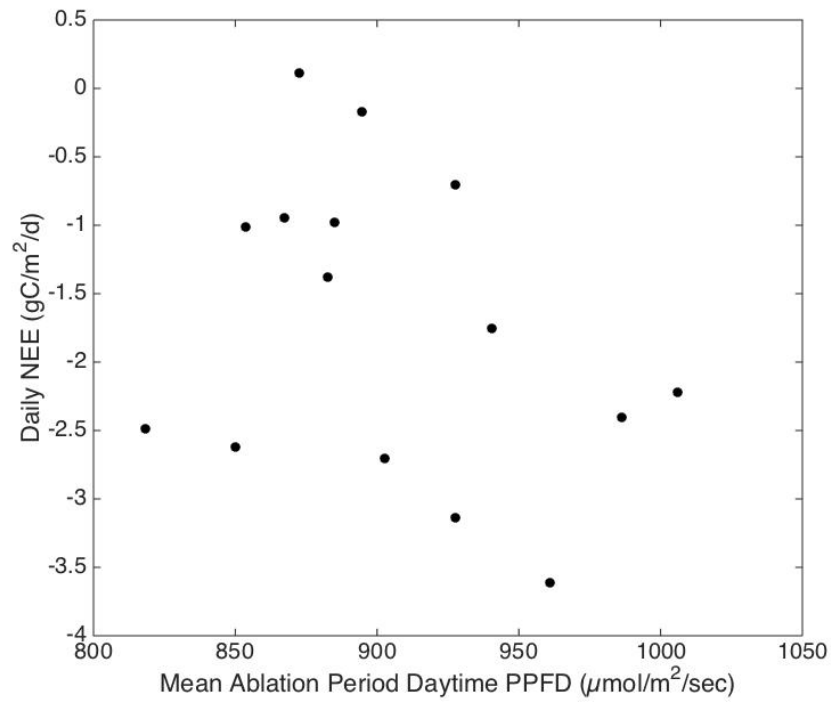


Figure A1 | Relationship between the mean ablation period daytime PPFD (horizontal axis) and the ablation period daily NEE (vertical axis) ($R^2=0.11$, $P=0.23$).

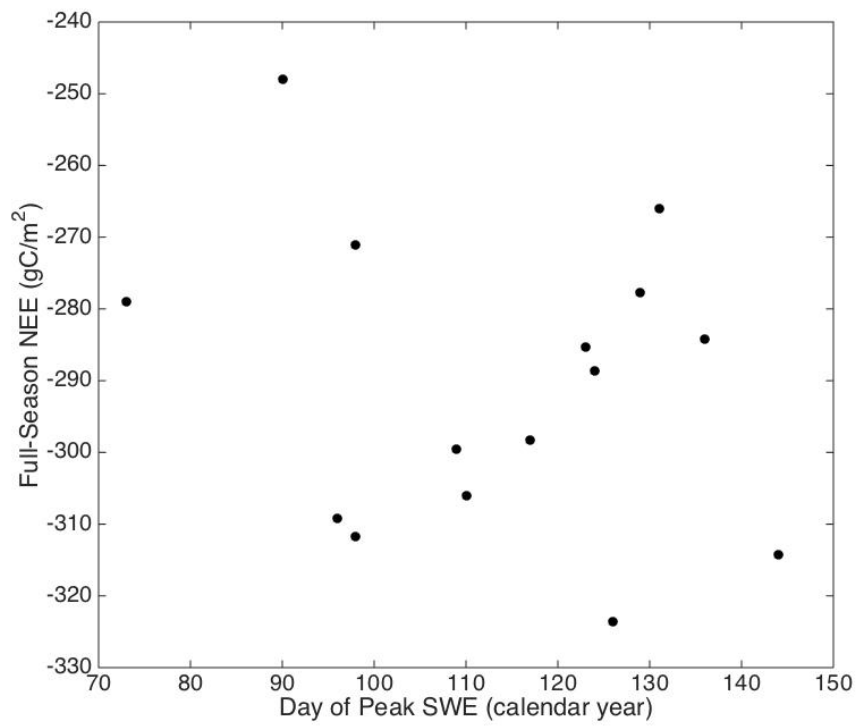


Figure A2 | Relationship between day of peak SWE (horizontal axis) and full-season NEE (vertical axis) ($R^2=0.06$, $P=0.39$).

Year	Peak SWE (m)	Ablation Period Start Date (DOY)	Ablation Period End Date (DOY)	Ablation Period NEE (gC/m ²)	Ablation Period Mean Air Temperature (°C)	Ablation Period Mean Daytime PPFD (μmol/m ² /sec)	Ablation Period Mean Daytime Net Radiation (W/m ²)	Last Day of Non-Ablation Period (DOY)
1999	0.3734	124	156	-56.21	3.70	940.7	387.1	304
2000	0.3175	96	138	-41.04	3.79	885.0	282.5	304
2001	0.2438	126	144	-48.62	5.98	902.8	320.9	309
2002	0.1753	90	121	3.36	1.91	872.6	342.3	295
2003	0.4013	98	153	-55.82	3.80	853.8	328.7	303
2004	0.2870	123	144	-54.96	6.57	850.1	326.8	298
2005	0.3251	129	148	-42.18	6.61	1006	364.8	305
2006	0.3150	98	137	-27.56	3.28	927.8	343.9	288
2007	0.4547	117	154	-92.02	4.96	818.3	311.7	307
2008	0.3785	109	154	-42.52	2.63	867.2	327.9	309
2009	0.4064	110	145	-48.16	4.21	882.7	343.5	293
2010	0.3023	136	153	-40.84	6.61	986.4	384.0	308
2011	0.4293	144	164	-72.29	7.92	961.2	374.8	301
2012	0.2769	73	127	-9.22	3.11	894.7	337.8	296
2013	0.4242	131	157	-81.57	6.71	927.6	361.9	289

Table A1 | 15 years of climate and snow ablation period data for the co-located Niwot Ridge AmeriFlux and SnoTel sites